Design of an in-wheel motor for a solar-powered electric vehicle

Article *in* IEE Proceedings - Electric Power Applications · October 1998

DOI: 10.1049/ip-epa:19982167 · Source: IEEE Xplore

3 authors, including:

Howard C. Lovatt
The Commonwealth Scientific and Industrial Research Organisation
86 PUBLICATIONS **932** CITATIONS
SEE PROFILE

B.C. Mecrow
Newcastle University
188 PUBLICATIONS **7,201** CITATIONS
SEE PROFILE

Design of an in-wheel motor for a solar-powered electric vehicle

H.C.Lovatt
V.S.Ramsden
B.C.Mecrow

Indexing terms: Solar power, Electric vehicles, In-wheel electric motor

Abstract: The design of an in-wheel electric motor for the solar-powered vehicle 'Aurora', entered in the 1996, 3010km Darwin – Adelaide World Solar Challenge solar car race is described. Compared to other entrants in the race, the brushless DC motor is more efficient (97.5% compared to 92–95%) and lighter (8.3kg compared to 12–16kg) than all other direct-drive motors, and more efficient than all motor/gear combinations. This is achieved by the use of high flux-density rare-earth magnets, and computer aided optimisation of an axial-flux configuration consisting of a Halbach magnet array and an ironless air-gap winding.

List of symbols

B = magnetic flux density
R = radius
ρ = resistivity
λ = length
ω = electrical frequency, rad/s
n = speed, rad/s

1 Introduction

The Darwin – Adelaide World Solar Challenge solar car race provides an ideal platform for the development of new high efficiency electric drives. There is very high expenditure on maximising the efficiency of the power generated by the solar cells, and minimising the aerodynamic, mechanical and electrical losses in the car. For a race car to remain competitive, its electric drive must also combine exceptionally high efficiency with low mass. The cost of the drive motor is a relatively small component of the overall race car cost, so that financial constraints do not significantly affect the design.

IEE Proceedings online no. 19982167

Paper received 18th March 1998

H.C. Lovatt is with CSIRO Telecommunications and Industrial Physics, PO Box 128, Lindfield, NSW 2070, Austrralia

V.S. Ramsden is with the Faculty of Engineering, University of Technology, Sydney, PO Box 123, Broadway, NSW 2007, Australia

B.C. Mecrow is with the Department of Electrical and Electronic Engineering, University of Newcastle upon Tyne, NE1 7RU, UK

To win the race a car needs to convert the maximum amount of solar energy, and use this energy well. The solar cell efficiency (24% from the University of New South Wales) and the race rules limit the available power to about 1.8kW for a single-seater car. A well designed solar powered race car can potentially average 100km/h at 1.8kW. In contrast, a typical road car, driven at this speed by an internal combustion engine, uses about 35kW from the engine and about 140kW from the fuel.

The losses incurred in mechanical gearing are excessively high, so direct drives have become the preferred alternative. These were first used in the World Solar Challenge in 1993 by three teams: Honda, Engineering College of Biel, and Northern Territory University [1]). Several other teams followed in 1996 [2]. The Aurora Vehicle Association introduced a novel 'wing section' car shape in 1993, which required a single front wheel and two rear wheels, rather than the more common reverse configuration with two wheels at the front [3].

Most of the 1.8kW generated in the solar car is used in overcoming aerodynamic drag and rolling resistance, with typically 5–10% lost in the electrical drive system. If the electrical losses were to be reduced to 2–3% it would give a key advantage in the race. This provided the motivation for the present work: design and test results of a very efficient, light-weight, direct-drive, in-wheel motor, ultimately placed in the single front wheel of the Aurora solar car are presented (Fig. 1). The efficiency of the motor was optimised, incorporating a mass penalty to allow for tyre rolling resistance. Cost was not considered in the design.

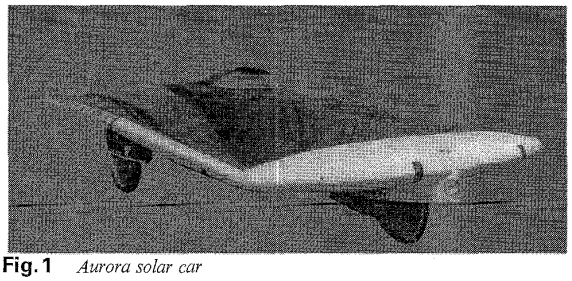

Fig. 1 *Aurora solar car*

2 Specification

The specification was initially for two motors, mounted in the rear wheels, with no fixed limit on overall mass. Direct drive was required to eliminate drive-train losses and each motor was required to fit inside a wheel to

reduce aerodynamic drag and maximise efficiency. However, initial work revealed that the complete specification could be met with a single motor of no more than six kilograms active mass. This motor was estimated to have full load losses of less than 56W, giving an efficiency of over 97%. This produced a much simpler, lighter system than a two motor drive, and became the preferred option. The motor could fit in the front wheel, allowing simple steering without upsetting the car stability at high speed. Based around this preliminary work a detailed specification was created, and is summarised in Table 1.

Table 1: Specification

Continuous output power	1800W
Peak power for 72s (hill climb)	3.1 × 1800W
Mean speed at 100, km/h	1060 rev/min
Max. speed at 130, km/h	1380 rev/min
Continuous torque	16.2Nm
Peak torque (hill climb)	50.2Nm
Starting torque	50.2Nm
Maximum outside diameter	360mm
Maximum axial length	43mm
Maximum active mass	6kg
Mass penalty	0.75W/kg

Note that there were two factors associated with wheel mass: the first was a maximum value beyond which stability of the car is compromised, with the front wheel starting to lift on rough roads at high speed. The second factor was a penalty with regard to increased rolling resistance and reduced acceleration as the mass increases. This latter penalty was expressed as an effective loss per kilogram of additional mass, but was only 0.75W/kg. Thus, even at the maximum mass of 6.0kg it remained a rather small penalty function in the overall design.

The specification called for a continuous torque per unit active mass of at least 3.24Nm/kg, which was more than double the value previously achieved by the other direct-drive motors used in the solar-powered race. It was also more than double the torque density achieved by a typical induction motor of similar rating (but of much lower efficiency). The torque per unit volume had to exceed 3700Nm/m^3, which was an equally high requirement.

Efficiency had to be maximised throughout the speed and power range, so that the car was able to continue to perform well under all conditions. This required minimisation of all load-independent losses, in order to maintain efficiency even in cloudy conditions, when the power generated was substantially reduced.

3 Machine type

Permanent magnet machines give a combination of high torque density and high efficiency because a high electric loading can be obtained, and no magnetising current losses are incurred. Thus they became the main contenders for this application. Inability to control the field flux meant that iron losses could not be reduced at light load. It was therefore important to produce a design with low hysteresis and eddy current loss to maintain efficiency across the power range.

The available envelope within the front wheel had a relatively large diameter, with a short axial length of only 12% of the diameter. The available space could contain a machine of well over 6.0kg, so that only a portion of the volume was to be actively used. However, it remained desirable to continue to use the maximum available radius, so that the magnetic forces were acting at a large radius, thus giving the maximum torque per unit mass. Consequently, the machine structure was chosen to form a ring, with a hole at the centre. This structure is commonly encountered in large, high torque machines, when inertia is not a significant problem.

3.1 Pole number

The choice of pole number was particularly important in this machine design. A high pole number was desirable for the following reasons:

- A large proportion of a typical machine mass comprises the flux return path. This mass is inversely proportional to the pole number.
- A high pole number was required to reduce the endwinding length and space. This was especially important when the machine had a relatively short stack length. It can easily be shown that with less than 30 poles in this machine the endwinding length was much greater than the active length, thus imposing a lower limit on the pole number.

These arguments must be balanced against the following issues which become important as the pole number (and therefore electrical frequency) rises:

- There is an increase in iron losses in all stationary iron components.
- There is a rise in eddy current losses in any air-gap windings.
- For a given air-gap length the magnet pole-pole leakage fields rise.
- There is an increase in the converter switching frequency, and therefore a reduction in converter efficiency.

From a practical viewpoint, it should also be noted that as the pole number rose, the dimensions of each pole reduced, so that the machine was composed of more small components and became difficult to assemble. A 60-pole design had a pole pitch of the order of 14mm and a maximum electrical frequency of 690Hz. This electrical frequency was found to impose a maximum limit on the possible pole number.

3.2 Machine geometry

Radial designs: In order to ascertain whether a radial field machine was feasible it was necessary to consider the endwinding space required. At the maximum of 60 poles, the pole pitch was approximately 14mm, and a similar amount of space was required at each end of the machine to accommodate the axial portion of the endwinding. The total available axial space was 43mm, thus leaving only 15mm for the active length. This length was too short for a competitive design, so that the radial field machine was abandoned.

Axial designs: There were a number of possibilities for an axial field design. Some designs [4, 5] had a single rotor and stator. However, such designs had several thousand newtons of axial pull on the bearings and were not favoured. If the axial forces were to be balanced, then either a single rotor, sandwiched between

two stators, or a single stator, sandwiched between two rotors was required [6]. The double stator option required more stationary iron than the double rotor one, and thus had greater iron loss. The double rotor design was therefore chosen. This design also had several mechanical advantages, as it became possible to mount each of the two rotors on the side walls of the wheel.

The pros and cons of an air-gap winding are relatively complex. In general terms an air-gap winding had the following advantages:

- For a given depth of slot there was more space available for the winding;
- A toothed structure was likely to have high tooth flux densities, and therefore a relatively high iron loss;
- For a given set of loadings the mass was reduced if there were no teeth present;
- A toothed structure was difficult to laminate in an axial field machine.

However, there were the following disadvantages:

- A poorer thermal performance when the winding was deep;
- A lower flux density for a given depth of magnets;
- Significant winding eddy current loss.

Optimisation of toothed structures revealed a rather large mass of teeth and a large iron loss. Unless the machine was constructed with a glassy metal core [7], the losses were calculated to exceed 80W in total. It was also found that with special magnet arrangements in an air-gap winding design it was possible to achieve peak air-gap flux densities of over 0.8T. This was as high as that typically achieved with a toothed structure, so that an air-gap winding became the preferred choice, providing that the thermal performance was adequate and the eddy current loss was kept low. Work proceeded with an air-gap winding design.

Even with an air-gap winding design there were two choices:

(i) A winding wound toroidally round a laminated core, with all air-gap fields returning circumferentially through the core [8–10].

(ii) An ironless stator with all flux passing axially through the stator (the brushless analogue of the disc armature DC motor).

The toroidal core machine had the advantages of high winding utilisation (the endwindings were short) and a relatively strong mechanical structure. However, the mass of the iron core was substantial and core iron loss significant. Optimisation of this design indicated that a 60-pole machine with a mass of 6.0kg, containing a glassy metal core, would have a core mass of about 1.2kg and a core loss of about 2.6W.

The ironless stator machine was predicted to have a similar performance to the glassy metal machine. Although construction of the stator winding assembly was difficult, the ironless stator had the major advantage that there were no forces on the stator during assembly of the machine. This was particularly important, as the stator was likely to be mounted onto a structure with a poor axial rigidity. Difficulty of assembling and annealing the glassy metal core within the limited time scale permitted for the project resulted in a decision to adopt the ironless stator topology.

In summary, an arrangement featuring axial flux, an ironless air-gap winding, and outer rotating magnets was selected for the following reasons:

Axial flux was chosen because:

- there was inadequate axial length for end windings in a radial-field air gap winding design;
- double magnet rotors could be mounted on the wheel side walls;
- the stator winding could be mounted centrally on the axle.

An *air-gap winding* was chosen because:

- the efficiency with toothed structures was less than 96%, due to tooth iron loss;
- a high field was still achievable with new permanent magnet materials and special magnet arrangements;
- more space was available for copper, leading to lower copper loss;
- eddy current loss was controllable with stranded Litz wire, leading to an efficiency greater than 97%.

An *ironless stator* was chosen because:

- The performance was similar to that calculated for a stator with a glassy metal core, which would be difficult to assemble and anneal;
- The mass was minimised for a given air-gap flux;
- There were no forces on the stator during assembly;
- The thermal performance was adequate.

The machine structure formed a ring with permanent magnet excitation for low losses, as shown in Fig. 2.

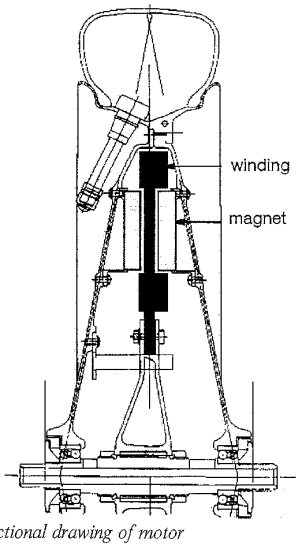

Fig. 2 *Cross-sectional drawing of motor*

4 Magnet arrangement

It was found that the maximum air-gap flux density per unit rotor mass could be achieved by means of a solid magnet rotor with no back iron, in an arrangement often called a 'Halbach' assembly [11], shown in Fig. 3. In such an arrangement, the magnets are oriented along the direction of the flux flow, so that in the interpolar region the magnets are magnetised circumferentially. This arrangement is particularly attractive for high pole configurations with air-gap windings. Performance is generally improved at the expense of

increased magnet volume and cost. Optimisation predicted that a design with the Halbach magnet arrangement would have approximately 10W (20%) less loss than an equivalent conventional arrangement of the same total mass, with magnets on backing iron.

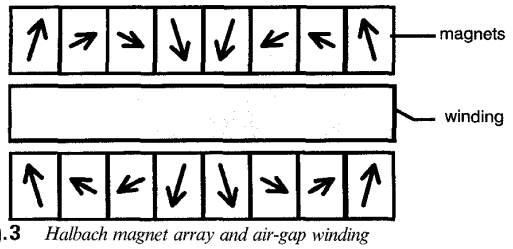

Fig. 3 *Halbach magnet array and air-gap winding*

In the ideal case the orientation of the magnets changes continuously with position, but in practice a finite number of magnets per pole must be used. The design chosen was found to give very good performance with four magnets per pole. When more magnets were used, only marginal increase in performance was possible. The angle of magnetisation of each magnet was varied, and optimised using search routines embedded in the finite element analysis. Best performance was produced with magnets at angles of 30° and 60° with respect to the axial direction.

5 Sources of loss

In the chosen motor design the only sources of loss are:

- winding copper loss,
- eddy current loss in the winding,
- windage loss,
- bearing loss.

Copper loss was the dominant source of loss in the three phase, fully pitched air-gap winding. The torque produced for a given excitation current was calculated using a virtual displacement method within the finite element simulation. From knowledge of the rated torque, the required MMF magnitude and resulting copper loss was determined.

The loss P_e resulting from eddy currents in a round conductor of radius R, resistivity ρ, and length λ, placed in a pulsating magnetic field of peak flux density B and frequency ω is [12]

$$P_e = \frac{\pi B^2 \omega^2 R^4 \lambda}{8\rho} \quad (1)$$

It was assumed that eddy current loss only occurs in the active portion of the winding. To reduce eddy loss, the winding was made of Litz wire with twisted (transposed) strands to reduce circulating currents.

The internal windage was also calculated from an analytical formula, which determines from the Taylor number that for this machine the flow regime is laminar with vortices. External windage was assumed to be the same as for a wheel without the motor, and so was not included. As there were no axial forces, bearing losses were also assumed to be the same as for a wheel by itself; these were not included either.

6 Design optimisation

The design was optimised to minimise the total loss. The optimisation initially used lumped parameter models, and later used 2-D finite-element analysis. The following assumptions were made:

- The heat transfer coefficient between the winding and the surrounding air was $20 Wm^{-2}K^{-1}$;
- Cooling was neglected for peak torque heating;
- There was no significant radial variation of magnetic field in the winding, i.e. no end effects. A 3-D finite-element solution indicated that this would not cause major errors;
- The air-gap magnetic field was effectively sinusoidal. This was confirmed by EMF measurement and flux density calculation.

The mass penalty of $0.75 W kg^{-1}$ was incorporated into the optimisation process.

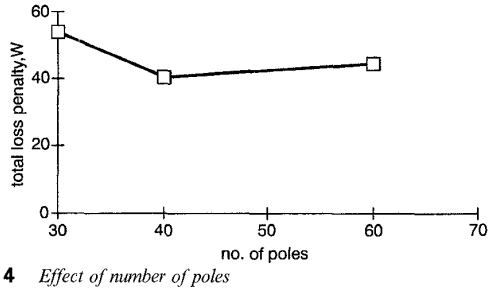

Fig. 4 *Effect of number of poles*

6.1 Choice of pole number

As discussed above, between 30 and 60 poles was initially thought to be sensible for this machine design. Optimisation results shown in Fig. 4 suggested that there was a small reduction in total loss penalty as the pole number was reduced from 60 to 40 poles, due to a reduction in eddy current loss, but that any further reduction caused a substantial increase in total penalty. This arises due to the increasing size of the endwindings and flux return paths. A 40-pole design has a pole pitch of the order of 21mm and a maximum electrical frequency of 460Hz, both of which are suitable values.

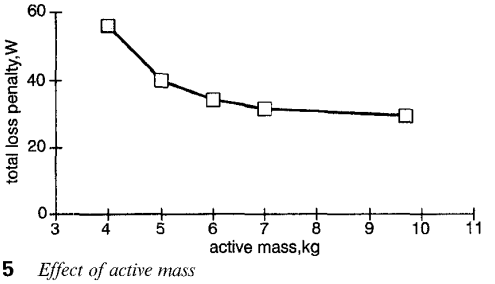

Fig. 5 *Effect of active mass*

6.2 Effect of mass

Fig. 5 shows how the total loss penalty is influenced by machine mass, with the machine fixed at 40 poles. It became clear that within the permissible mass range, any increase in mass resulted in a net gain, despite the mass penalty of 0.75W/kg. Thus it became clear that the optimal design would sit at the the upper limit of mass, in this case 6.0kg.

6.3 Effect of air-gap length

The effect of air-gap length is shown in Fig. 6. Although the loss penalty could be reduced by up to 5W with an air-gap length below 2.0mm, the gap was

kept at 2.0mm on each side of the winding to allow for winding encapsulation and mechanical clearance.

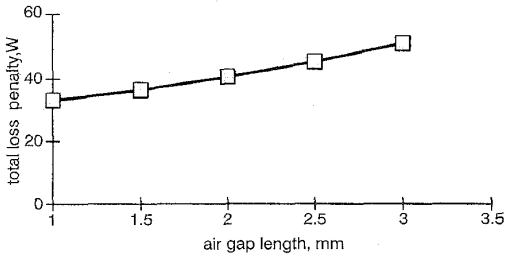

Fig. 6 *Effect of air-gap length*

7 Design results

Some further design results obtained for the 6.0kg motor are shown in Tables 2 and 3. The magnet selected was VAC362HR, a neodymium iron boron material, with B_r = 1.33T at 20°C.

Table 2: Design results

Mass of copper	1.2kg
Mass of magnets	4.78kg
Total active mass	5.98kg
Mass penalty	4.5W
Peak air-gap flux density (20°C)	0.91T
Winding	2-layer, fully pitched
RMS current density	3.12A/mm^2
Total force of attraction on rotor faces	4900N

Table 3: Comparison of design and measured results for 6kg motor at 16.2Nm, 1060 rev/min, 1800W, 20°C

	Design	Motor 2
Axial gap between magnet rotors, mm	9.3	10.0
Phase resistance, Ω	0.0723	0.0997
RMS fundamental phase current, A	9.6	11.34
LN RMS EMF, V	61.9	54.3
EMF constant (LN RMS EMF/speed, rad/s)	0.56	0.47
Torque constant per phase, Nm/A	0.56	0.49
Copper loss, W	20.0	38.6
Eddy current loss, W	4.6	2.7
Windage (design for 2mm gap each side), W	0.4	2.1
Total loss, W	25.0	43.4
Efficiency (%)	98.6	97.9
Temperature rise, K	10.2	18.3
Temp. rise after a further 72s at 50Nm, K	37.5	42
Temperature rise at 30Nm, K	30.0	60

Two motors were fabricated. A magnet ring is shown in Fig. 7 and a stator winding in Fig. 8. The stator was naturally air cooled. The final total weight was 8.3 kg including magnet carriers, stator encapsulation, central support and terminations.

8 Experimental results

Tests were conducted to determine the motor resistance, inductance, EMF constant, EMF waveform, torque constant, no-load losses, load losses, efficiency and temperature rise.

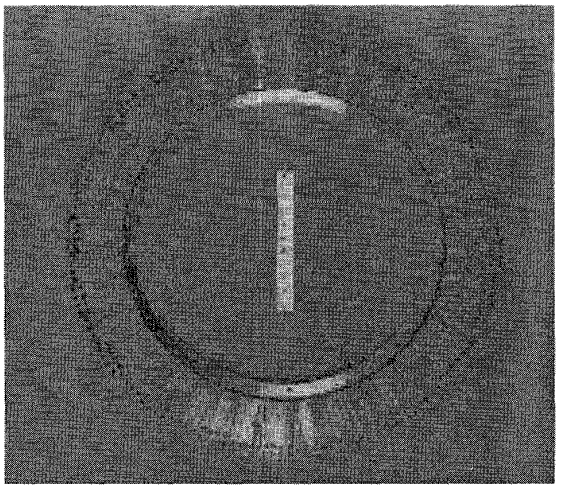

Fig. 7 *Magnet ring*

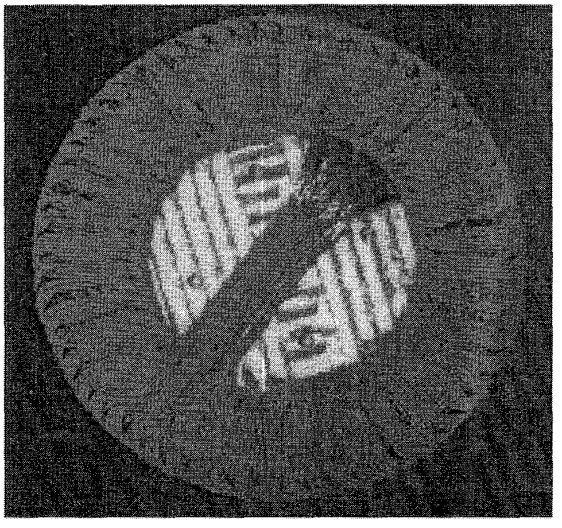

Fig. 8 *Stator winding*

8.1 No-load tests

The no-load losses were separated by a series of retardation tests, as follows:

(i) with the magnets and stator removed to reveal bearing loss and external windage;

(ii) with dummy magnets and the stator inserted to give the internal windage;

(iii) with the actual magnets replaced, thus adding the winding eddy current loss.

The results are shown below and graphed in Fig. 9:

External windage = $1.25 \times 10^{-5} n^3$ W

Bearing loss = $0.002n + 0.00033n^2$ W

Internal windage = $1.5 \times 10^{-6} n^3$ W

Winding eddy loss = $0.00022n^2$ W

It can be seen that the major no-load loss is the external windage (17W at nominal speed 1060 rev/min), followed by the bearings (5W at nominal speed), both of which are not included in the motor losses. The inter-

nal windage was 2.1W and winding eddy loss 2.7W. The internal windage was more than the estimated value of 0.4W (for 2mm gap each side) due to winding encapsulation, and the eddy loss lower than the estimated value of 4.6W, but fortuitously the sum was approximately as estimated.

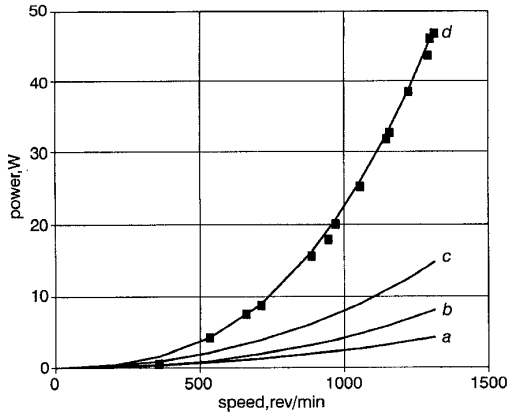

Fig. 9 *No load loss breakdown from retardation tests compared with no-load test as a motor*
a Eddy loss in windings
b Eddy loss plus internal windage
c Eddy loss, internal windage plus bearings
d Total loss from retardation tests (Eddy loss, internal windage, bearings plus external windage)
■ Total loss from no load motor test

The open circuit line-neutral EMF constant measured during the third retardation test was 0.47V/(rad/s), 16% lower than the estimated value of 0.56V/(rad/s). This indicates a reduced flux linkage, and largely explains the lower winding eddy loss (proportional to B^2 as shown in eqn. 1). The magnet flux density profile has not yet been measured to determine the cause of the flux decrease. But interestingly, it could be measured in an open motor, as there is no backing iron and the permeability of the rare earth magnet in the region of operation is close to 1.0, so the air gap flux density is the sum of that from the two magnet rings in isolation.

8.2 Load tests

Load tests were conducted by mounting the wheel between two shaft torque transducers (providing low friction bearings) and allowing the tyre to rest with the appropriate force on a rotating flywheel. The flywheel was then loaded with a DC generator, as shown in Fig. 10. Depending on the direction of rotation, one torque transducer output shaft was locked to react against the wheel motor.

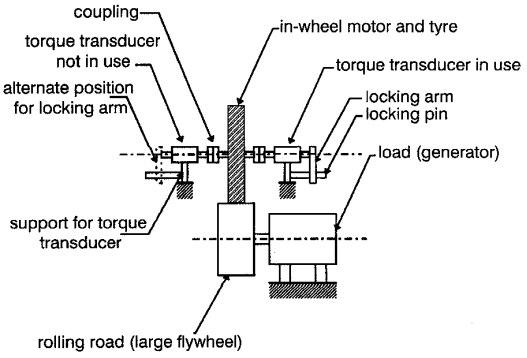

Fig. 10 *Load test rig*

During both load tests and in the actual race, the motor was supplied from a quasi-square-wave MOSFET inverter. The motor synchronous inductance was only 22μH (0.01p.u.) so external inductors of 100μH (0.05p.u.) per phase were used to limit the current ripple resulting from the switching action of the converter. The RMS value of the quasi-square-wave current was 5% higher than the ideal sine wave, leading to 10% extra copper loss (≈ 4 W), but saving some inverter switching loss.

Input power, voltage, current and supply frequency (speed) were measured with a calibrated Voltech PM3000A, 0–500kHz, 0.1% digital power analyser, and the torque transducers were calibrated Vibrometer TM series, 0.2%. The resistance was measured with a Cropico digital milliohmmeter.

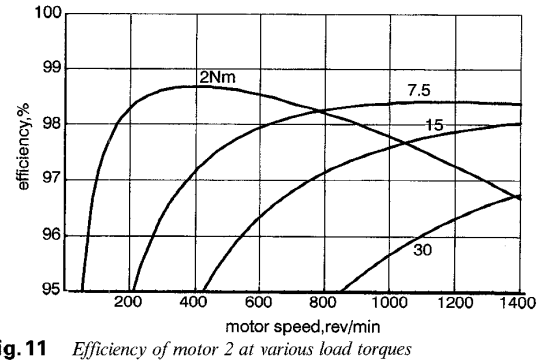

Fig. 11 *Efficiency of motor 2 at various load torques*

Some results for motor 2 are compared with design values in Table 3 (the corresponding efficiency of motor 1 was 97.5%), and the efficiency predicted from the measured results is plotted against speed in Fig. 11, with 10mΩ added to the phase resistance for leads and connections. The machine has almost 98% efficiency at rated torque and speed, but the winding resistive loss reduces the efficiency if this torque is maintained at lower speeds. At one half rated torque the machine exceeds 97% efficiency once above one quarter base speed. The copper loss was higher than expected due to the lower flux mentioned above, and due to a higher phase resistance. With more careful construction in future it should be possible to reduce the copper loss and approach the estimated efficiency.

Table 4: Comparison of Aurora motor at 30Nm with 30Nm, 950 rev/min induction motor and internal combustion engine and drive train

	Torque/total weight ratio	Torque/total volume ratio	Efficiency	Losses
	Nm/kg	Nm/m³	%	%
Aurora	3.61	10135	96	4
Induction	0.80	1500	82	18
IC engine	1.5	1970	25	75

The performance at 30Nm (the approximate thermal limit rating with natural cooling) is contrasted with that of a typical 30Nm, 6-pole induction motor and an internal combustion engine and drive train in Table 4. Compared with an induction motor, this machine produces over four times the torque per unit mass, and six times the torque per unit volume, with less than one quarter the losses. An inverter mass and volume should

strictly be added to give a fairer comparison with the IC engine.

Table 5: Comparison of Aurora performance with 1993 direct-drive solar car motors [1]

	Aurora	Honda	Biel	NTU
Total weight, kg	8.3	12.8	12.0	16.5
Nominal speed, rev/min	1060	1000	900	600
Nominal torque, Nm	16.2	14.3	14.9	22.3
Thermal limit torque, Nm	30	14.3	14.9	55.7
Nominal torque/total weight ratio, Nm/kg	1.95	1.12	1.24	1.35
Efficiency (%)	97.5	95	95	92

A further comparison is given in Table 5, with the earlier direct-drive solar car motors (The efficiency of the Biel motor is given in [1] as 97.5 % at 14.9Nm, 900 rev/min (1.4kW), but 1996 information from Storey gave this as 95%). The new Aurora motor has a lower mass and higher efficiency than all the other motors.

9 Conclusions

This report has detailed a motor design which has been optimised for high-efficiency, in-wheel operation. The design uses an axial field, air-gap winding in order to produce 1800W at 1060 rev/min, with 6.0kg of active mass at an efficiency of more than 97.5 %. The design is thermally suitable for twice the required rating. This design of motor is suitable for a range of applications where high specific output must be combined with very high efficiency.

10 Acknowledgments

The authors acknowledge the help and advice in motor and controller design, fabrication and testing given by: J. Dunlop, P. Gwan, and W. Wu at CSIRO; A. Curgenven, W. Holliday, and P. Watterson at UTS; G. Wilkinson; and the Aurora team, particularly S. Bicknell, M. Burns, G. Locock, and R. Simmonson. Financial support from CSIRO, UTS and Aurora is acknowledged.

11 References

1 STOREY, J.V.W., SCHINCKEL, A.E.T., and KYLE, C.R.: 'Solar racing cars 1993 world solar challenge' (Australian Government Publishing Service, Canberra, 1994)
2 ROCHE, D.M., SCHINCKEL, A.E.T, STOREY, J.V.W. HUMPHRIS, C.P. and GUELDEN, M.R.: 'Speed of light - the 1996 world solar challenge' (Photovoltaics Special Research Centre, University of New South Wales, Sydney, 1997)
3 BADDELEY, V., HUMPHRIS, C., and PUDNEY, P.: 'The Aurora Q1 solar-powered racing car'. Presented at ANZAAS Congress, Australia, 1994
4 'What's the Diff? 'Desert Rose' solar vehicle hub drive technology', *Australian Energy Management News,* June 1994,
5 DI NAPOLI, A., CARICCHI, F., CRESCIMBINI, F., and NOIA, G.: 'Design criteria of a low-speed, axial flux, PM synchronous machine'. Proceedings of international conference on *Evolution and modern aspects of synchronous machines*, 1991, Vol. 3, pp. 1119–1124
6 ZHANG, Z., PROFUMO, F., and TENCONI, A.: 'Axial-flux versus radial-flux permanent magnet-motors', *Electromotion,* 1996, **3**, pp. 134–140
7 JENSEN, C.C., PROFUMA, F., and LIPO, T.A.: 'A low loss permanent magnet brushless DC motor utilizing tape wound amorphous iron', *IEEE Trans. Ind. Appl.,* 1992, **28**, pp. 646–651
8 SPOONER, E., and CHALMERS, B.J.: 'Toroidally-wound, slotless, permanent-magnet, brushless DC motors'. Proceedings of ICEM'88, 1988, Vol. 3, pp. 81–86
9 SPOONER, E., and CHALMERS, B.J.: 'TORUS: a slotless, toroidal-stator, permanent-magnet generator', *IEE Proc. B,* 1992, **139**, pp. 497–506
10 CARICCHI, F., CRESCIMBINI, F., HONORATI, O., DI NAPOLI, A., and SANTINI, E.: 'Compact wheel direct drive for EVS', *IEEE Ind. Appl. Mag.,* 1996, pp. 25–32
11 OFORI-TENKORANG, J., and LANG, J.H.: 'A comparative analysis of torque production in Halbach and conventional surface-mounted permanent magnet synchronous motors'. IEEE IAS annual general meeting, Orlando, 1995, pp. 657–663
12 CARTER, G.W.: 'The electromagnetic field in its engineering aspects' (Longmans, 2nd ed., 1967), p. 254